

Soft Matter

Accepted Manuscript



This is an *Accepted Manuscript*, which has been through the Royal Society of Chemistry peer review process and has been accepted for publication.

Accepted Manuscripts are published online shortly after acceptance, before technical editing, formatting and proof reading. Using this free service, authors can make their results available to the community, in citable form, before we publish the edited article. We will replace this *Accepted Manuscript* with the edited and formatted *Advance Article* as soon as it is available.

You can find more information about *Accepted Manuscripts* in the [Information for Authors](#).

Please note that technical editing may introduce minor changes to the text and/or graphics, which may alter content. The journal's standard [Terms & Conditions](#) and the [Ethical guidelines](#) still apply. In no event shall the Royal Society of Chemistry be held responsible for any errors or omissions in this *Accepted Manuscript* or any consequences arising from the use of any information it contains.



Journal Name

ARTICLE

Probing dispersion and re-agglomeration phenomena upon melt-mixing of polymer-functionalized graphite nanoplates

R. M. Santos,^a C. Vilaverde,^a E. Cunha,^a M. C. Paiva^{a*} and J. A. Covas^a

Received 00th January 20xx,
Accepted 00th January 20xx

DOI: 10.1039/x0xx00000x

www.rsc.org/

A one-step melt mixing method is proposed to study dispersion and re-agglomeration phenomena of as-received and functionalized graphite nanoplates in polypropylene melts. Graphite nanoplates were chemically modified *via* 1,3 dipolar cycloaddition of azomethine ylide and then grafted with polypropylene-graft-maleic anhydride. The effect of surface functionalization on the dispersion kinetics, nanoparticle re-agglomeration and interface bonding with the polymer is investigated. Nanocomposites with 2 or 10 wt. % of as-received and functionalized graphite nanoplates were prepared in a small-scale prototype mixer coupled to a capillary rheometer. Samples were collected along the flow axis and characterized by optical microscopy, scanning electron microscopy and electrical conductivity measurements. As-received graphite nanoplates tend to re-agglomerate upon stress relaxation of the polymer melt. The covalent attachment of polymer to the nanoparticle surface enhances the stability of dispersion, delaying re-agglomeration. Surface modification also improves interfacial interactions and the resulting composites presented improved electrical conductivity.

Introduction

Nanostructures based on carbon allotropes – graphite, fullerenes, carbon nanotubes and graphene – are a versatile class of materials that are attracting substantial scientific and technological interest specially due to their remarkable mechanical and electrical properties¹. Their potential applications include single molecule gas detection², actuators and supercapacitors³, transparent conducting electrodes⁴, corrosion prevention⁵, drug delivery and tissue engineering⁶, biomaterials⁷ and polymer nanocomposites⁸⁻¹².

Graphite, formed by stacks of 2-D layers of sp² hybridized carbon atoms hexagonally bonded, with open edges, is a promising low cost (naturally abundant) reinforcement for functional and smart nanocomposites^{8, 9, 13}. Its in-plane stiffness (Young's modulus) is approximately 1 TPa, and its electrical ($\approx 10^6 \Omega \cdot \text{cm}^{-1}$) and thermal conductivity ($\approx 400 \text{ W} \cdot \text{m}^{-1} \cdot \text{K}^{-1}$) are also exceptional¹⁴. It has been theoretically predicted that graphite has an edge-inherited non-bonding π -state (combination of zigzag and armchair edges) at about the Fermi level, in addition to the π bonding and π^* antibonding states, resulting in unconventional magnetic features¹⁵.

However, in practice, the incorporation and dispersion of natural flaky graphite in polymer matrices is challenging due to the strong interaction and small spacing between graphene layers (0.335 nm center-to-center, generating an interstitial space of much less than 0.3 nm)¹⁶ and lack of functional groups at the surface and edges¹⁷. The former hinders polymer

intercalation in-between layers and their exfoliation, while the latter deters the creation of strong interfacial bonding with the polymer.

Exfoliated graphite can be synthesized by various methods, including intercalation with a alkali metal, a alkali earth metal, a rare earth metal for donors and metal halides, halogen and acids for acceptors^{8, 18, 19}. Most of the graphite flakes obtained by these procedures, usually denoted as graphite nanoplates (GnP)²⁰, have a thickness from 0.34 to 100 nm²¹. Intercalation increases the interlayer spacing and weakens mutual interactions, facilitating exfoliation by mechanical, thermal or microwave techniques¹⁶.

Chemical modification of GnP has been accomplished by non-covalent or covalent approaches to overcome the limitations associated to the efficient dispersion and interfacial bonding with polymers^{2, 22, 23}. Non-covalent modification through electrostatic interactions, Van der Waals forces, hydrogen bonding or π - π stacking interactions enables the attachment and stabilization of diverse functional groups (e.g. proteins, DNA-protein complexes, organic supermolecules) at the surface of the graphitic lattice without disturbing the electronic network²⁴. Covalent functionalization generally encompasses two routes: addition of free radicals or dienophiles to carbon-carbon bonds and formation of covalent bonds between functional groups and oxygen groups present in graphite oxide. Some of the most attractive organic species for chemical reactions with sp² carbons of graphite are highly reactive free radicals formed by the diazonium addition reaction, and the 1,3 dipolar cycloaddition (DCA)²³ of azomethine ylides. This versatile reaction has been successfully applied in the functionalization of fullerenes²⁵, carbon nanotubes²⁶, carbon nanofibers²⁷ and graphene, as it accesses

Institute for Polymers and Composites/13N, University of Minho, Campus de Azurém, 4800-058 Guimarães, Portugal
*corresponding author: mcpaiva@dep.uminho.pt

a variety of organic derivatives by selecting the appropriate aldehyde and α -amino acid as precursor, depending on the required applications (polymer composites, drug delivery and nanoelectronic devices)²⁸. The covalent bond presents the advantage of generating stronger interfaces with the polymer, and better withstand the processing conditions in comparison with non-covalent approaches²⁹.

An overview of literature reveals that functionalization of conductive carbon nanoparticles plays an important role in widespread applications and commercialization of nanocomposites¹⁷. Chemical modification enhances dispersion and interfacial interactions with the polymer³⁰⁻³² and prevents re-agglomeration^{32,33}. In this work, graphite nanoplates were functionalized *via* 1,3 dipolar cycloaddition and then grafted with polypropylene-graft-maleic anhydride (PP-*g*-MA). The kinetics of their dispersion in a Polypropylene (PP) matrix, as well as the stability of the morphology generated under quasi-steady conditions, were studied and compared with the equivalent behaviour of the as-received graphite. The experiments were performed using a prototype small-scale mixer that generates a strong extensional flow component^{34,35} and is fixed to a capillary rheometer in order to induce flow under well controlled conditions. Moreover, it allows for material sampling along its axis, thus providing the possibility of monitoring the evolution of dispersion. Polypropylene nanocomposites with 2 and 10 wt. % of as-received and chemically modified GnP were prepared under identical conditions. The progression of nanoparticle dispersion along the mixer length was evaluated by optical and scanning electron microscopies; the electrical conductivity of the composites was measured. GnP re-agglomeration effects upon melt relaxation were analyzed.

2 Experimental section

2.1 Materials

Polypropylene copolymer, Icorene CO14RM[®] from ICO POLYMERS, with a melt flow index of 13.1 g/10 min (190 °C, 2.16 Kg) and a density of 0.9 g/cm³ was used as polymer matrix. PP-*g*-MA containing 8 – 10 wt. % of maleic anhydride, with a weight-average molecular mass (Mw) of approximately 9.1 Kg/mol and a density of 0.934 g/cm³ was supplied by Sigma-Aldrich. According to the manufacturer (XG Sciences, Inc.), graphite nanoplates xGnP[®] Grade C-750 has a thickness of approximately 2 nm, an average diameter of less than 2 μm and a typical average surface area of 750 m²/g. They were supplied in powder form, and the powder particle projected area was assessed by dilution of the powder in an epoxy resin, spreading on glass slides and measuring by optical microscopy. The flakes of the two fillers (GnP and *f*GnP-PP) generate agglomerates whose particle size distribution is revealed in Figure 1. It was computed from the analysis of at least 70 images of each, with a total measured area of agglomerates of 6.7×10^5 and $4.9 \times 10^5 \mu\text{m}^2$ for as-received and *f*GnP-PP, respectively. While the larger agglomerate (maximum agglomerate area) was in the range of $2.5 - 3.0 \times 10^4 \mu\text{m}^2$, the average

agglomerate size was 1.1×10^4 and $7.2 \times 10^3 \mu\text{m}^2$ for the as-received and functionalized GnP, respectively.

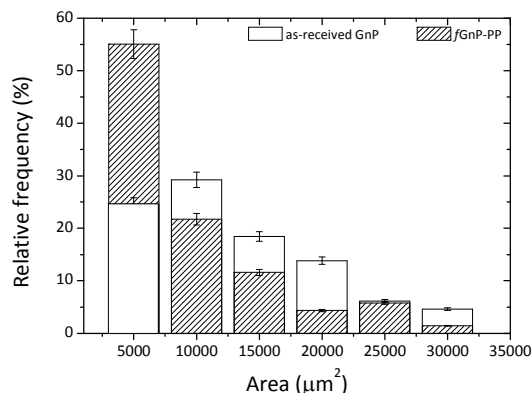


Fig. 1 – Particle size distribution of as-received GnP and chemically modified *f*GnP-PP (powder form) before melt mixing.

2.2 Functionalization of graphite nanoplates

The as-received graphite nanoplates were chemically modified *via* 1,3 dipolar cycloaddition of azomethine ylides generated *in-situ* by thermal decomposition of paraformaldehyde (analytical grade, from Sigma-Aldrich) and reaction with *N*-benzyloxycarbonylglycine (from Sigma-Aldrich) at 250 °C for 3 hours, yielding functionalized GnP (*f*GnP), under a procedure similar to that described for the functionalization of carbon nanotubes³⁶. Figure 2 summarizes the steps involved in the preparation of *f*GnP and *f*GnP-PP.

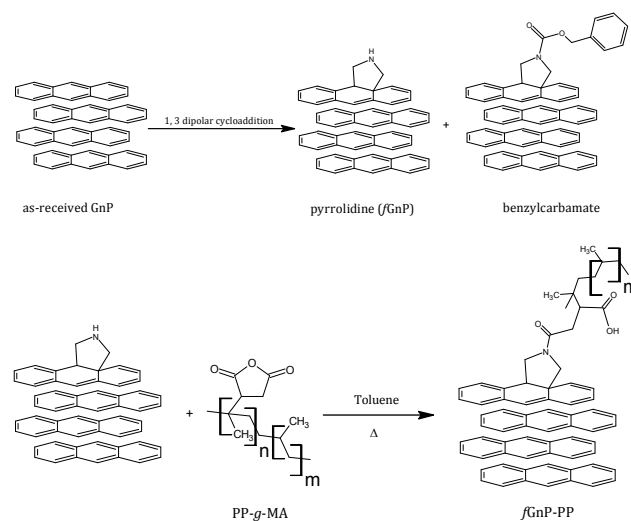


Fig. 2 – Functionalized graphite nanoplates after DCA reaction and grafting with PP-*g*-MA.

PP-*g*-MA was then grafted onto the *f*GnP surface yielding PP-functionalized GnP (*f*GnP-PP). The reaction was carried out by

refluxing the *f*GnP in a solution of PP-*g*-MA (1:2 molar ratio) in toluene for 3 hours, under magnetic stirring. The resulting suspension was filtered, followed by repeated washing with hot toluene and dried overnight in a vacuum oven at 100 °C.

2.3 Production of nanocomposites

The nanocomposites were manufactured by forcing a premix of polymer plus filler - by means of the descending ram of a capillary rheometer - through a mixer containing a series of circular channels with alternating small/large diameters, thus inducing repetitive convergent/divergent flows. It is well established that the normal stresses created superimposed on the shear stress field are particularly effective for dispersion^{35, 37, 38}. Changing the dimensions and/or number of channels, ram speed and temperature creates a wide range of flow conditions. Similarly to what has been observed for carbon nanotubes^{35, 39}, graphite nanoplates seem to re-agglomerate once the thermomechanical stresses applied to achieve dispersion are relieved⁴⁰. This morphology instability has obvious practical implications, considering the similitude to the usual industrial practice of manufacturing polymer-based nanocomposites by twin-screw extrusion, followed by processing of the final composite part, either by melt processing in a single screw extruder or in a plasticising unit of an injection moulding equipment. The composite production step usually generates higher hydrodynamic stresses compared to the final processing step. Thus, the possible occurrence of this phenomenon was also investigated by appending a circular channel with a larger diameter after the mixer; in turn, the evolution of a second dispersion operation could also be studied by attaching a second series of circular channels with alternating diameters. The resulting layout is represented in Figure 3.

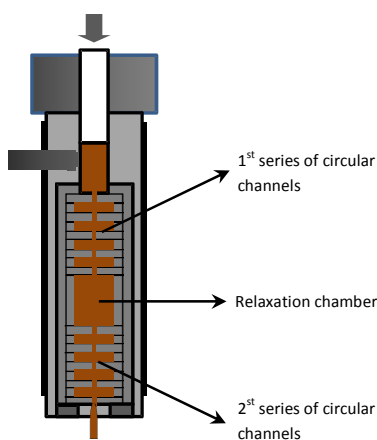


Fig. 3 – Schematics of the configuration of the prototype small-scale mixer used to prepare PP nanocomposites with as-received GnP and chemically modified *f*GnP-PP.

The mixer consists of a sequence of ten circular channels having different internal diameters, *d* (equal to 8 and 1 mm and lengths of 2 mm), inducing an 8:1 convergence, followed by a relaxation chamber (*d* of 18 mm and length of 24 mm) and another similar sequence of ten circular channels. Each individual channel is shaped by a circular ring, the entire flow configuration consisting of a vertical stack of rings assembled inside a sleeve. The latter can be quickly unscrewed from the main body of the mixer, in order to provide access to the material inside each channel. After pre-heating the mixed polymer-GnP powders at 200 °C for 5 min the melt was forced through the channels of the mixer at 50 mm.min⁻¹, corresponding to an average shear rate of approximately 1500 s⁻¹ in the smaller capillary channel, 3.0 s⁻¹ in the larger channel and 0.3 s⁻¹ in the relaxation chamber. Once each experiment was concluded, the set-up was removed from the rheometer and samples were collected, cooled in N₂ (l) and dried with air.

2.4 Characterization

2.4.1 Graphite nanoplates

Thermogravimetric analysis was performed in a Modulated TGA Q500 (TA instruments) heating under constant nitrogen flow (60 mL.min⁻¹) from 100 to 750 °C at a rate of 10 °C. min⁻¹. X-ray photoelectron spectroscopy (XPS) was carried out in a Thermo Scientific K-Alpha ESCA instrument equipped with Al-Kα_{1,2} monochromatized radiation (1486.92 eV). The base pressure in the chamber was maintained at about 3 × 10⁻⁹ mbar. Photoelectrons were collected at an angle perpendicular to the sample surface. A constant analyzer energy mode (CAE) was used with a pass energy of 100 eV and 20 eV for the survey spectra and high resolution spectra, respectively. Charge referencing was done by setting the lower binding energy C1s photo peak. The atomic percent (at. %) compositions were determined from the survey XPS spectra considering the integrated peak areas using the Shirley background subtraction method and the Scofield sensitivity factors. Core level curve fitting was performed using a convolution of a Lorentzian function (describing 1s hole lifetime effect) with a Gaussian function (temperature-dependent phonon broadening).

Optical microscopy of as-received and chemically modified GnP (in powder form) was carried out on a BH2 Olympus microscope coupled to a Leica DFC 280 camera to characterize the initial particle size distribution before melt compounding. For this purpose, 10.0 mg of GnP were gently dispersed in 4.25 mL of epoxy resin, then spread onto a glass slide and dried at room temperature for 24 h.

As-received and chemically modified GnP were also dispersed in a butyl alcohol solution (1.2 g.L⁻¹) under sonication (CREST 230T ultrasonic bath, 80 W) for 2 hours at room temperature and then directly deposited onto a cooper grid for subsequent observation by transmission electron microscopy (TEM) on a JEOL JEM1010, equipped with a CCD Orius camera and a tungsten filament as electron source, at an acceleration voltage of 100 kV.

2.4.2 Nanocomposites

The extent of dispersion of GnP in the PP matrix was estimated from quantitative particle size analysis. Composite sections with 5 μm thickness were cut with a Leitz 1401 microtome at room temperature, using glass knives with an angle of 45°. Optical micrographs were acquired with a Leica DFC 280 digital camera coupled to a BH2 Olympus microscope using a 20x objective and 1.6x ocular magnification. The agglomerate areas were measured using the Leica Application Suite 4.4. software. At least five composite sections were analyzed, each one with the total area of $3.5 \times 10^5 \mu\text{m}^2$. The parameters selected to quantitatively describe the state of GnP dispersion were the agglomerate area ratio (A_r), the total number of agglomerates per unit area (N) and the area of the largest agglomerate in the subset of the smaller agglomerates that constitute 50 or 90% of the total area. A_r is the fraction of composite area occupied by agglomerates, calculated as the ratio of the sum of the areas of all n agglomerates measured divided by the total composite area analyzed (A_T):

$$A_r = \frac{\sum_{i=1}^n A_i}{A_T} \times 100 \% \quad (1)$$

A cumulative distribution of the agglomerate areas, described as a function of the agglomerate area (CA_j) was evaluated according to:

$$CA_j = \frac{\sum_{i=1}^j A_i}{\sum_{GnP} A_i} \times 100 \% \quad (2)$$

i.e., by summing the area of the individual agglomerates i in ascending area order ($\sum_{i=1}^j A_i$) and dividing by the total agglomerate area ($\sum_{GnP} A_i$). The size of the larger agglomerate contained in 50 % ($A_{x,50}$) and 90 % ($A_{x,90}$) of the total agglomerate area was obtained from the cumulative distribution of agglomerate areas, CA_j .

The morphology of cryo-fractured nanocomposites sputtered with a gold/palladium mixture was examined by scanning electron microscopy (SEM) on a NanoSEM – FEI Nova 200, operating at an accelerating voltage of 5.00 KV in backscattering electro image mode, coupled to an energy dispersive X-ray (EDAX- Pegasus X4M) spectrometer. The dielectric properties of the nanocomposites were measured on the disk-shaped samples extracted from the mixer, using a Quadtech 1920 Precision LCR meter. Measurements were performed at a voltage of 1V and a frequency ranging from 500 Hz to 1 MHz, at room temperature. The dielectric cell consisted of parallel plates having 3 mm diameter electrodes that were gold coated on the sample surface by magnetron sputtering. Four measurements were carried out for each sample, the average values being reported here. The real part of the electrical conductivity was calculated by:

$$\sigma'(\omega) = \omega \epsilon_0 \epsilon''(\omega) \quad (3)$$

where ω is the angular frequency, ϵ_0 is the permittivity in vacuum and $\epsilon''(\omega) = \epsilon' \tan \delta$ is the imaginary part of permittivity, where $\tan \delta$ is the dissipation factor and ϵ' is the real part of permittivity⁴¹.

3 Results and discussion

3.1 Graphite nanoplates functionalization

The thermal degradation of as-received and chemically modified graphite nanoplates was compared by means of thermogravimetry, in order to confirm the presence of organic groups bonded through the DCA reaction. The variation of weight with temperature and its first derivative are shown in Figure 4 a) and b), respectively.

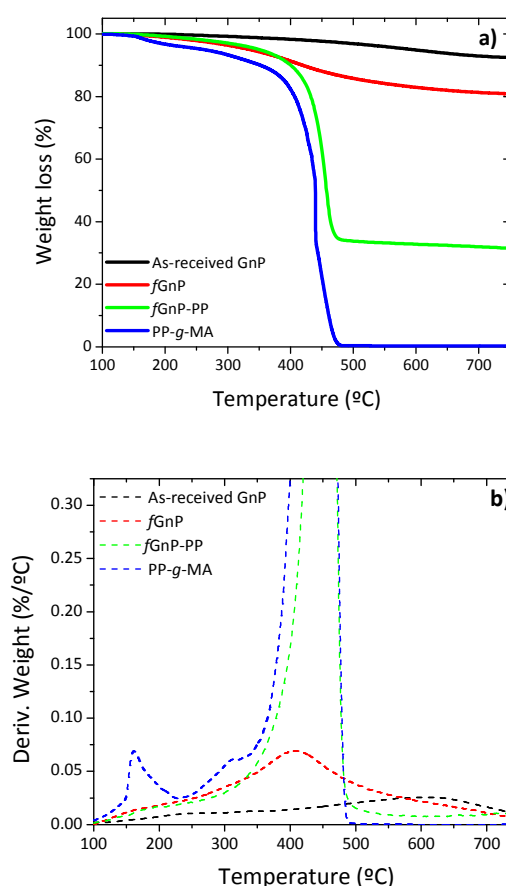


Fig. 4 - TGA of PP-g-MA and as-received and chemically modified GnP; a) TGA curves; b) First derivative of TGA curves.

The thermal degradation of as-received GnP shows a minor weight loss of approximately 3 % up to 500 °C, due to the elimination of adsorbed compounds and residual oxidation. The first derivative evidences a broad band with low intensity that may be ascribed to the elimination of CO₂ and CO (from

150 to 350 °C), hydroxylic or phenol functionalities (in the range of 350 - 500 °C) and carbonaceous impurities (at circa 600 °C)^{38, 39}. After carrying out the DCA reaction, *f*GnP are characterized by a weight loss of 14 % from 150 to 500 °C, with higher decomposition rate near 400 °C, assigned to the elimination of the covalently bonded organic groups (pyrrolidine or benzylcarbamate represented in Figure 2). A further increase of weight loss is observed for *f*GnP-PP, near 52.5 %, indicating that a large uptake of PP-*g*-MA took place. The PP-*g*-MA shows two degradation steps near 150 and 300 °C, corresponding to the thermal decomposition of the grafted maleic anhydride (MA) groups. These degradation steps are absent in the TGA of *f*GnP-PP, confirming that most of the MA moieties grafted onto PP reacted with the pyrrolidine groups at the surface of *f*GnP, forming strong covalent bonds.

Additional evidence of functionalization of the GnP surface was obtained by XPS spectroscopy, as shown in Figure 5. The atomic nitrogen and oxygen content at the surface of as-received and chemically modified GnP are presented in Table I.

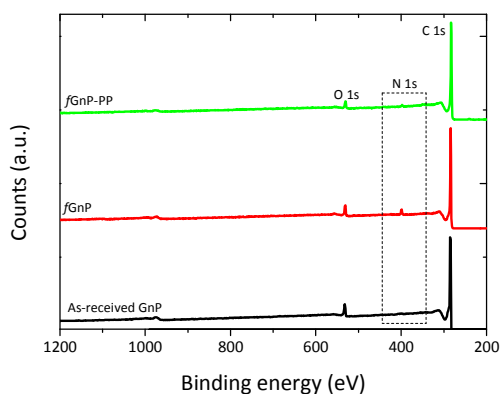


Fig. 5 - XPS survey spectra of as-received and chemically modified graphite nanoplates.

The atomic nitrogen and oxygen content at the surface of as-received and chemically modified GnP are presented in Table I. The strong peak at 284.9 eV, common to as-received and functionalized GnP, was attributed to the conjugated carbon atoms in the graphitic lattice (C 1s). The signal near 532 eV was ascribed to oxygen atoms (O1s) incorporated during thermal expansion⁴² for the as-received GnP. After the DCA reaction, the N 1s peak appears at approximately 400 eV, confirming the presence of nitrogen-containing functional groups²². The survey spectrum of *f*GnP provides a surface composition of 3.31 at. % of N, and a similar oxygen content as the original GnP (Table I). Besides confirming bonding of N-containing functional groups to the GnP surface, this result indicates that these functional groups are mostly in pyrrolidine form, as the presence of benzylcarbamate would increase the overall oxygen content.

Table I - Surface chemical elemental composition of as-received and chemically modified GnP.

Graphite nanoplatelets	Surface chemical elemental composition (at. %)				
	C	O	N	S	N/C ratio
As-received GnP	93.94	5.95	0.11	---	0.001
<i>f</i> GnP	90.84	5.50	3.31	0.30	0.040
<i>f</i> GnP-PP	94.72	4.14	1.14	---	0.012

The analysis of the background-corrected high resolution C1s core level XPS region of the as-received and chemically modified graphite nanoplates is presented in Figure 6.

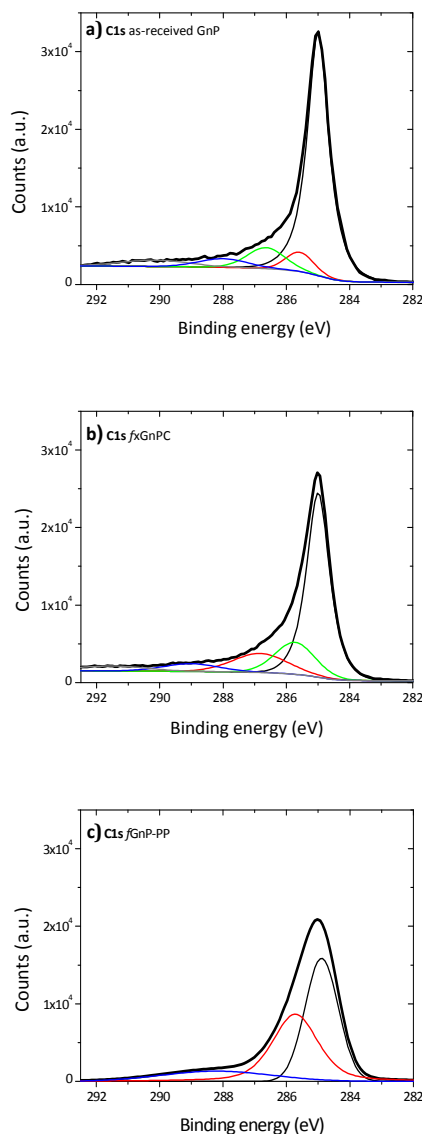


Fig. 6 – Background-corrected high resolution C 1s core level XPS region of as-received (a) and functionalized (b) and c) graphite nanoplates.

The deconvolution of the C 1s peak of as-received GnP shows two contributions above 286 eV (green) and near 288 eV (blue), attributed to carbon atoms singly bonded to an oxygen atom – alcohol or ether (-COR) – and to carbonyl (-C=O) groups, respectively⁴³. A small component peak shifted 0.5 eV to higher binding energy relative to sp² C-C bonds (red) may be assigned to sp³ C-C bonds. An area increase of this component peak was observed for *f*GnP and may be associated with the presence of -CH₂- and C-N of the cyclic pyrrolidine. After reaction with PP-*g*-MA, a large increase of this component peak area was observed. The C1s peak becomes broad and is mainly composed by two contributions centered near 285 and

285.5 eV, with a ratio of approximately 6:5. Thus, either the grafted PP covers part of the *f*GnP surface, or the PP layer is thin and allows the detection of the GnP sp² carbon. A new small component peak centered at 288.2 eV is observed, which may be assigned to amide or imide bonds (O=C-N) formed by reaction of maleic anhydride and pyrrolidine.

TEM images (Figure 7) depict as-received GnP as thicker flakes compared to *f*GnP, demonstrating that the DCA reaction does not induce nanoparticle destruction, but may induce some exfoliation. After reaction with PP-*g*-Ma, the morphology is apparently maintained.

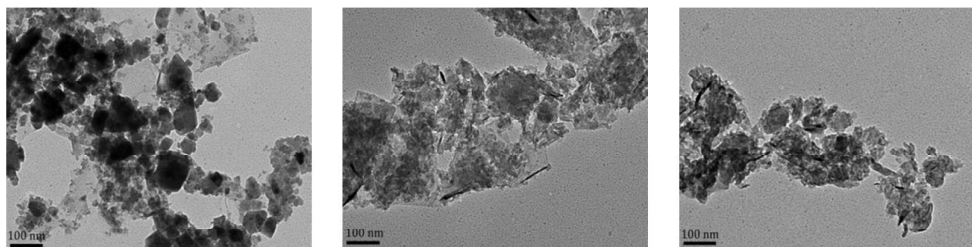


Fig. 7 - TEM images of: a) as-received GnP, b) *f*GnP and c) *f*GnP-PP.

3.2 Dispersion of graphite nanoplates

Optical micrographs illustrating the morphology of PP nanocomposites with 2 and 10 wt. % of as-received GnP and

*f*GnP-PP at various locations along the mixer are depicted in Figure 8.

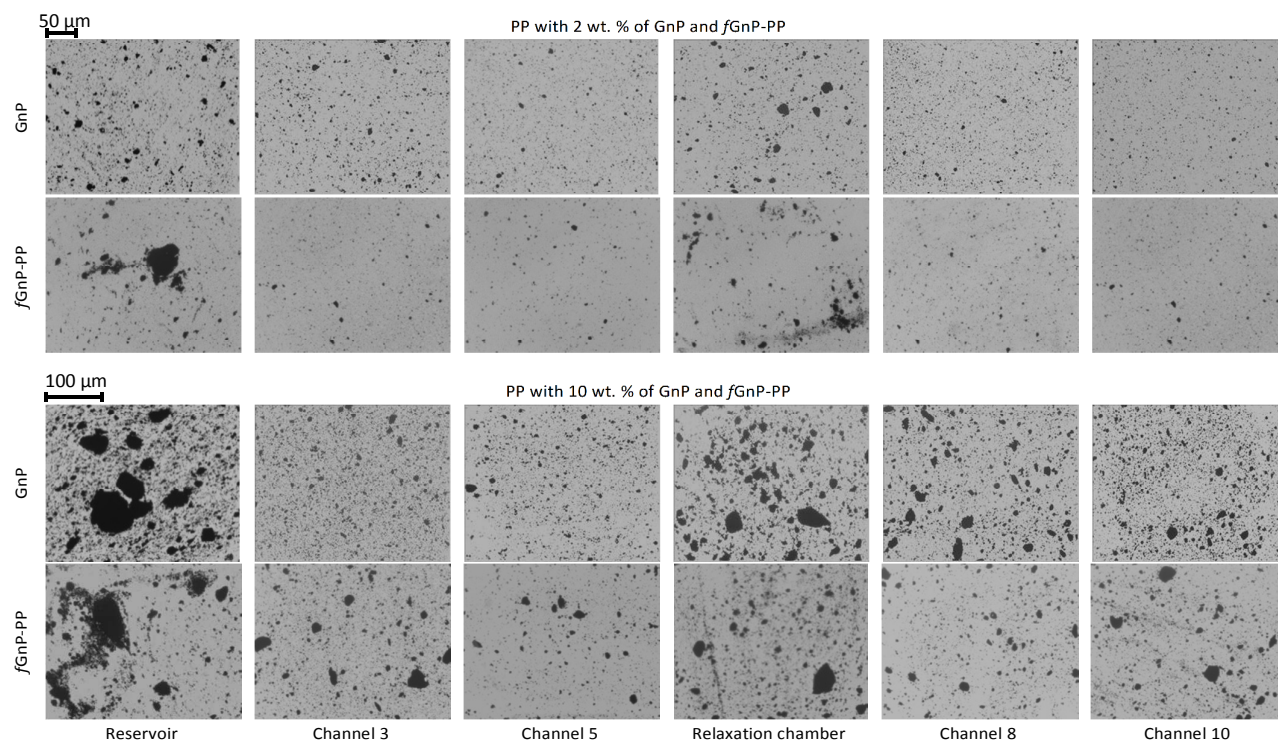


Fig. 8 - Morphology development of PP nanocomposites with 2 and 10 wt. % of as-received GnP and *f*GnP-PP at various locations along the mixer.

The agglomerate morphology was imaged at the reservoir of the capillary rheometer, channels 3 and 5 of the first mixing zone, relaxation zone, and channels 8 and 10 of the second mixing zone (the equivalent to channels 3 and 5 of the first mixing zone). Regardless of filler content, a significant decrease of the GnP agglomerate size is revealed from the reservoir to channel 5, thus demonstrating the efficiency of extensional flow to induce dispersion. At the relaxation chamber, where the applied shear stress is small (the shear rate is approximately 0.3 s^{-1}), the area of the GnP agglomerates increase, suggesting that re-agglomeration took place. In the second mixing zone dispersion sets in again, the morphology at channel 10 approaching that at channel 5. Figure 9 displays SEM images of the nanocomposites with 2 and 10 wt. % of GnP and *f*GnP-PP removed from channel 5, illustrating the typical morphology of the agglomerates at the end of the first mixing section. In all cases, SEM shows that the agglomerates appear as composite areas of high GnP concentration, i.e., they are not constituted solely by GnP.

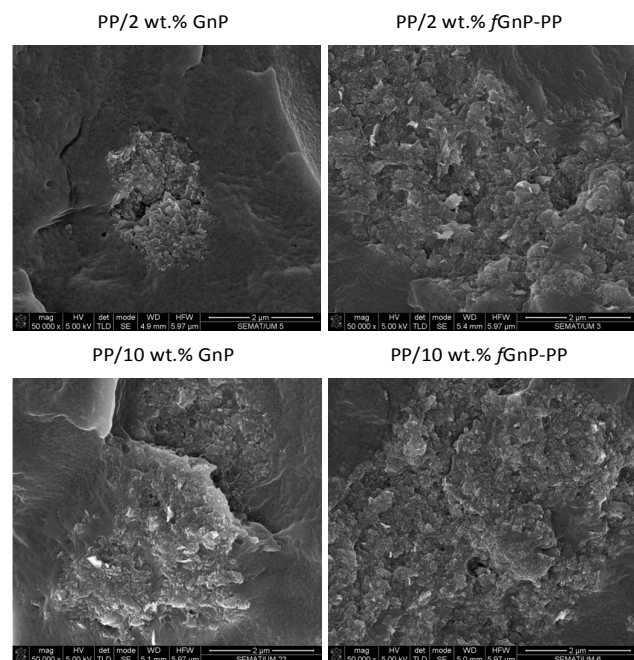


Fig. 9 – SEM micrographs of PP nanocomposites containing 2 and 10 wt. % of as-received GnP and chemically modified *f*GnP-PP removed from channel 5.

A quantitative assessment of the evolution of GnP and *f*GnP-PP dispersion in the PP matrix along the mixer, as described by

relevant statistical parameters, is provided in Figure 10 and Table II. A_{x50} and A_{x90} represent the area of the largest agglomerate in the subset of the smaller agglomerates that constitute 50% or 90% of the total (Σ_{GnP}), respectively.

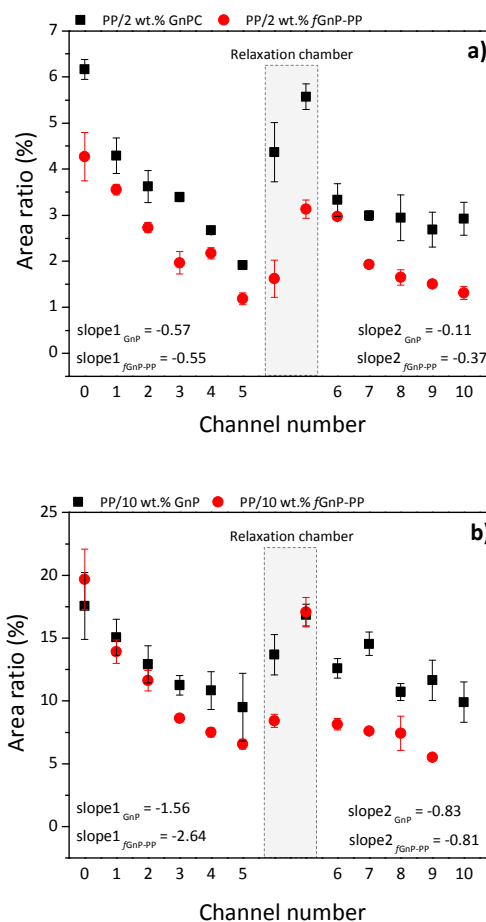


Fig. 10 – Evolution of A_x along the extensional mixer for PP nanocomposites with a) 2 and b) 10 wt. % of as-received GnP and chemically modified *f*GnP-PP, respectively.

Their evolution along the mixer shows a consistent dispersion of GnP agglomerates along the first mixing zone, a re-agglomeration stage in the relaxation chamber and a subsequent dispersion sequence in the second mixing zone. It should be noted that the material collected at the reservoir upstream of the mixer already evidenced some dispersion, the average particle size reducing approximately one order of magnitude relative to the original value.

Indeed, for as-received GnP the average size of $6.7 \times 10^5 \mu\text{m}^2$ decreased to 1.5×10^4 and $5.2 \times 10^4 \mu\text{m}^2$ for the composite concentrations of 2 and 10 wt. % GnP, respectively, whilst for the functionalized filler the corresponding values are $4.9 \times 10^5 \mu\text{m}^2$, 1.2×10^4 and $4.8 \times 10^4 \mu\text{m}^2$, respectively. At constant filler concentration, Table II shows that the number of agglomerates per unit area (mm^2), N , is typically smaller for the composite comprising *f*GnP-PP. The final N for the nanocomposites with 2 and 10 wt. % of *f*GnP-PP was 1278 and 1763, respectively, while the nanocomposites with 2 and 10 wt. % of as-received GnP contained 1766 and 4439, respectively.

Figure 10 analyzes the evolution along every channel of the mixer of A_r , a dispersion parameter commonly used in the literature^{17, 39, 44, 45}, showing consistently higher values for the as-received GnP compared to *f*GnP-PP. Hence, the amount of individually dispersed nanoplates (not detectable by optical microscopy) must be larger for the composite with *f*GnP-PP. The composites demonstrate a nearly linear progression of dispersion along the first mixing zone, indicating that the process is influenced by residence time.

Manas-Zloczower and co-workers^{46, 47} postulated that the mechanism of dispersion (rupture *versus* erosion) of agglomerated particles in a melt depends on the magnitude of

the fragmentation number, which is defined by the ratio between hydrodynamic stresses and cohesive strength of the agglomerate, as well as on a finite probability for break-up, which is proportional to residence time and agglomerate surface area. Thus, at constant stress, the smaller the agglomerate the longer the exposure time required to break it. As for the rate of dispersion, it should increase with the intensity of the hydrodynamic stresses generated. This is confirmed in Figure 10, which shows that the slope of the A_r variation along the mixer in the first mixing zone is almost 3 times greater for the system containing 10 wt. % GnP compared to 2 wt. % GnP, which may be explained by the higher viscosity expected for the composite with 10 wt. % GnP. In fact, Table III shows an increase in the total pressure measured for the composite with 10 wt. % GnP relative to the composite with 2 wt. % GnP, consistent with a viscosity increase. Pressure is directly proportional to shear stress and thus to viscosity, since shear rate remains constant. For the composites with *f*GnP-PP, Table III shows a decrease in the total pressure relative to GnP and even to the neat polymer (for 10 wt. %), which is indicative of lower viscosity. This could be a consequence of slippage of the polymer melt on the surface of the polymer-grafted graphite nanoplates⁴⁸.

Table II - Assessment of dispersion of as-received GnP and functionalized *f*GnP-PP in the PP matrix.

Set-up	$A_{x50} (\mu\text{m}^2)$	$A_{x90} (\mu\text{m}^2)$	N per unit area (mm^{-2})	$A_{x50} (\mu\text{m}^2)$	$A_{x90} (\mu\text{m}^2)$	N per unit area (mm^{-2})
	PP/2 wt.% GnP			PP/2 wt.% <i>f</i> GnP-PP		
Reservoir	26.0	240.7	4106	173.9	2000.3	1749
Channel 3	22.6	152.2	2199	38.9	273.38	1648
Channel 5	15.9	74.90	1057	29.4	131.5	1183
Relaxation chamber	25.5	167.4	3819	70.4	634.0	1120
Channel 8	24.4	139.5	1617	40.0	279.1	1375
Channel 10	17.8	88.5	1766	29.7	191.3	1278
	PP/10 wt.% GnP			PP/10 wt.% <i>f</i> GnP-PP		
Reservoir	236.3	6328.0	6418	1940.9	8729.5	3026
Channel 3	29.8	515.5	6774	131.9	997.4	4379
Channel 5	26.3	220.3	5456	88.5	886.2	3230
Relaxation chamber	244.2	1585.7	2108	149.3	1977.0	3641
Channel 8	59.5	651.8	4586	171.1	1222.3	3026
Channel 10	44.6	297.6	4439	179.7	701.8	1763

ARTICLE

Table III – Pressure measured at the rheometer entrance (ram speed of 50 mm.min⁻¹).

Nanoparticle	Nanoparticle content in the composite (wt.%)	Pressure (MPa)
-	0	17.1
GnP	2	18.3
	10	24.3
<i>f</i> GnP-PP	2	17.2
	10	14.1

Thus, considering again the definition of fragmentation number, and given the smaller hydrodynamic stresses generated at lower viscosity, the improvement in dispersion (lower A_r) observed for the composites with *f*GnP-PP can only be attributed to a significant decrease in the agglomerate cohesion. In fact, the PP molecules chemically bonded to the surface of the *f*GnP-PP increase the equilibrium distance between neighbouring GnP, thus considerably decreasing the Van der Waals interactions responsible for the cohesion of their agglomerates.

Once the composites enter the relaxation chamber, the hydrodynamic (shear) stresses become lower than the cohesive forces and enough residence time is provided to allow progressive re-agglomeration, eventually yielding agglomerates with an A_r approaching the value measured at the reservoir. This type of phenomenon was reported before for the melt mixing of carbon nanotubes with polymers^{35, 39} and remains a major practical difficulty to their widespread use, since practical manufacturing sequences often require re-melting of the melt-mixed composites and processing by another method. GnP functionalization had a limited success in stabilizing the morphology of the nanoplates in the relaxation chamber, although the data shows a slower re-agglomeration pace.

Dispersion of the two types of filler regains its approximate linear progression in the second mixing zone, albeit at a smaller pace and after a more abrupt reduction of A_r at the 6th channel. The values of A_r for the composites with chemically modified filler remain consistently smaller than those for composites with as-received filler. For the composite with 2 wt.% of as-received GnP, the A_r measured after the 10th channel (exit of the second mixing section) is larger than after the 5th channel (exit of the first mixing section). All remaining composites reached similar A_r values after the 5th and 10th channels. It should be noticed that, for all composites, the slope of A_r variation in the second mixing section is considerably smaller than that measured along the first mixing section, which is surprising since the first and second mixing sections have exactly the same design, generating the same residence time and average shear rate. In terms of

fragmentation number, this means that lower hydrodynamic stresses were generated in the second mixing section and/or the cohesive strength of the agglomerates increased from the first to the second mixing sections. While the former is not obvious to account for, the morphology and/or cohesion of the agglomerates formed upon re-agglomeration in the relaxation chamber could be different from that of the agglomerates at the reservoir of the capillary. Agglomerates consisting of smaller particles loosely attached to each other, but appearing as large agglomerates under the optical microscope, may be generated. In the second mixing zone, the small agglomerates will quickly detach from each other, but the probability of further rupture is lower (under similar flow conditions). This effect is schematically depicted in Figure 11. Differences between as-received and chemically functionalized GnP should again be attributed to differences in nanoplate-nanoplate interactions and slippage of the polymer melt at the nanoparticle polymer-grafted surface. Further studies need to be carried out to extensively characterize the evolution of agglomerate morphology along the dispersion system.

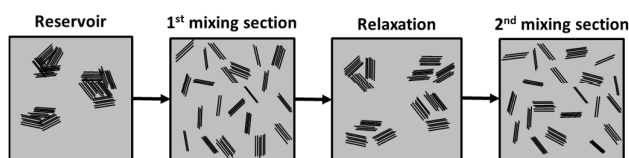


Fig. 11 - Schematic representation of a possible evolution of GnP agglomerates in PP (grey area), along the mixer.

The electrical conductivity of polymer-based nanocomposites is known to be strongly dependent on filler size, loading, shape, surface modification and degree of dispersion⁴⁹. The variation of AC conductivity with frequency for neat PP and its nanocomposites is presented in Figure 12.

The results illustrate the electrically insulating nature of PP, displaying increasing conductivity with increasing frequency, and a conductivity value of approximately 10⁻⁹ S.m⁻¹ at 1 kHz⁵⁰. After incorporation of 2 or 10 wt. % of as-received GnP (Figure 12a), the nanocomposites conductivity at 1 kHz increases to approximately 10⁻⁸ S.m⁻¹ and still displays a frequency-dependent behaviour, suggesting that the formation of a three-dimensional interconnecting network was not achieved. Nanocomposites with *f*GnP-PP (Figure 12b) show slightly higher electrical conductivity relative to the composites with as received GnP.

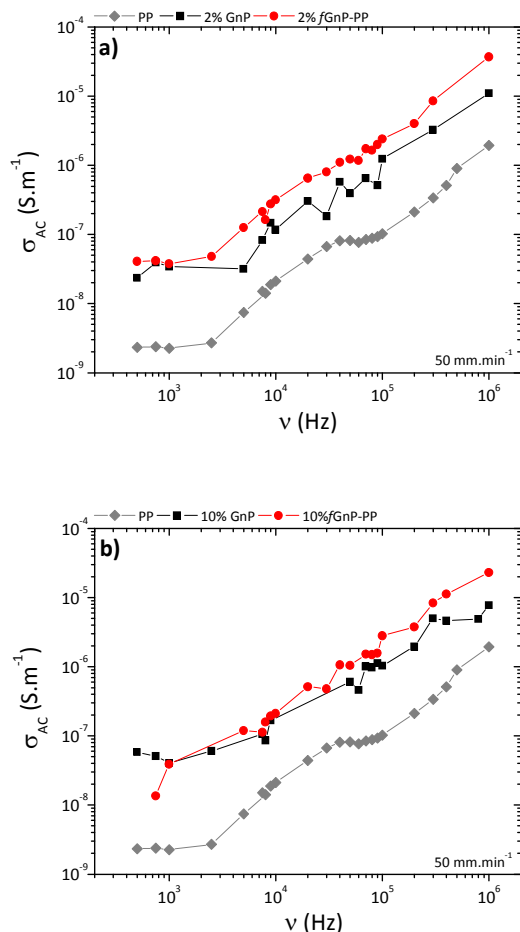


Fig. 12 – AC conductivity vs. frequency for neat PP and its nanocomposites with a) 2 and b) 10 wt. % of GnP and fGnP-PP.

Conclusions

Nanocomposites containing 2 or 10 wt. % of graphite nanoplates were prepared by melt mixing using a small scale intensive mixer coupled to a capillary rheometer. Regardless of filler loading, a significant decrease of the agglomerate size takes place, showing that extensional flow efficiently stimulates the dispersion of graphite nanoplates. At the relaxation chamber, where the shear rate is approximately 0.3 s^{-1} , a prominent increase of agglomerate area occurs, suggesting that re-agglomeration took place. The morphology and/or cohesion of these re-formed agglomerates seem to be different from that of the initial agglomerates at the reservoir of the capillary rheometer, affecting its subsequent dispersion rate in the second mixing zone. Surface modification of GnP with polymer enhances the stability of dispersion and delays re-agglomeration. A better GnP/polymer interface and enhanced electrical conductivity could also be noticed for nanocomposites containing functionalized graphite nanoplates.

Further advances in surface functionalization of GnP may contribute to the stability of the dispersed nanoparticles in the polymer melt. The magnitude of GnP re-agglomeration may be minimized by merging the steps of nanocomposite manufacture and processing into one single operation, avoiding its negative effects on performance.

Acknowledgements

The authors acknowledge the financial support to Project Matepro – Optimizing Materials and Processes, with reference NORTE-07-0124-FEDER-000037 by the Programa Operacional Regional do Norte (ON.2) and Portuguese Foundation for the Science and Technology (FCT) for PEst-C/CTM/LA0025/2013. EC acknowledges FCT for PhD grant SFRH/BD/87214/2012.

References

1. A. K. Geim and K. S. Novoselov, *Nat Mater*, 2007, **6**, 183-191.
2. V. Singh, D. Joung, L. Zhai, S. Das, S. I. Khondaker and S. Seal, *Progress in Materials Science*, 2011, **56**, 1178-1271.
3. U. K. Sur, *International Journal of Electrochemistry*, 2012, **2012**, 12.
4. P. Avouris, *Nano Letters*, 2010, **10**, 4285-4294.
5. E. P. Randviir, D. A. C. Brownson and C. E. Banks, *Materials Today*, 2014, **17**, 426-432.
6. S. Goenka, V. Sant and S. Sant, *Journal of Controlled Release*, 2014, **173**, 75-88.
7. W. G. Zheng, S. C. Wong and H. Sue, *J. Polymer*, 2002, **43**, 6767.
8. J. R. Potts, D. R. Dreyer, C. W. Bielawski and R. S. Ruoff, *Polymer*, 2011, **52**, 5-25.
9. R. J. Young, I. A. Kinloch, L. Gong and K. S. Novoselov, *Composites Science and Technology*, 2012, **72**, 1459-1476.
10. T. K. Das and S. Prusty, *Polymer-Plastics Technology and Engineering*, 2013, **52**, 319-331.
11. V. Dhand, K. Y. Rhee, H. Ju Kim and D. Ho Jung, *Journal of Nanomaterials*, 2013, **2013**, 14.
12. X. Huang, X. Qi, F. Boey and H. Zhang, *Chemical Society Reviews*, 2012, **41**, 666-686.
13. R. Sengupta, M. Bhattacharya, S. Bandyopadhyay and A. K. Bhowmick, *Progress in Polymer Science*, 2011, **36**, 638-670.
14. H. Kim and C. W. Macosko, *Macromolecules*, 2008, **41**, 3317-3327.
15. T. Enoki and Y. Kobayashi, *Journal of Materials Chemistry*, 2005, **15**, 3999-4002.
16. B. Z. Jang and A. Zhamu, *J Mater Sci*, 2008, **43**, 5092-5101.
17. P.-C. Ma, N. A. Siddiqui, G. Marom and J.-K. Kim, *Composites Part A: Applied Science and Manufacturing*, 2010, **41**, 1345-1367.
18. H. Selig and L. B. Ebert, in *Advances in Inorganic Chemistry and Radiochemistry*, eds. H. J. Emeléus and A. G. Sharpe, Academic Press, 1980, vol. Volume 23, pp. 281-327.
19. F. L. Vogel, US Patent 4,565,649, 21 January 1986.
20. A. Bianco, H.-M. Cheng, T. Enoki, Y. Gogotsi, R. H. Hurt, N. Koratkar, T. Kyotani, M. Monthieux, C. R. Park, J. M. D. Tascon and J. Zhang, *Carbon*, 2013, **65**, 1-6.

21. L. R. Bunnell, US Patent 5,186,919, 16 February 1993.
22. M. Quintana, K. Spyrou, M. Grzelczak, W. R. Browne, P. Rudolf and M. Prato, *ACS Nano*, 2010, **4**, 3527-3533.
23. V. Georgakilas, M. Otyepka, A. B. Bourlinos, V. Chandra, N. Kim, K. C. Kemp, P. Hobza, R. Zboril and K. S. Kim, *Chemical Reviews*, 2012, **112**, 6156-6214.
24. J. Liu, J. Tang and J. J. Gooding, *Journal of Materials Chemistry*, 2012, **22**, 12435-12452.
25. M. Maggini, G. Scorrano and M. Prato, *Journal of the American Chemical Society*, 1993, **115**, 9798-9799.
26. N. Tagmatarchis and M. Prato, *Journal of Materials Chemistry*, 2004, **14**, 437-439.
27. R. Araújo, F. Fernandes, M. Proença, C. Silva and M. Paiva, *Journal of nanoscience and nanotechnology*, 2007, **7**, 3441-3445.
28. P. A. Denis and F. Iribarne, *International Journal of Quantum Chemistry*, 2010, **110**, 1764-1771.
29. C. Klumpp, K. Kostarelos, M. Prato and A. Bianco, *Biochimica et Biophysica Acta (BBA) - Biomembranes*, 2006, **1758**, 404-412.
30. C. A. Mitchell, J. L. Bahr, S. Arepalli, J. M. Tour and R. Krishnamoorti, *Macromolecules*, 2002, **35**, 8825-8830.
31. J. Zhu, J. Kim, H. Peng, J. L. Margrave, V. N. Khabashesku and E. V. Barrera, *Nano Letters*, 2003, **3**, 1107-1113.
32. Y.-J. Wan, L.-C. Tang, D. Yan, L. Zhao, Y.-B. Li, L.-B. Wu, J.-X. Jiang and G.-Q. Lai, *Composites Science and Technology*, 2013, **82**, 60-68.
33. P.-C. Ma, S.-Y. Mo, B.-Z. Tang and J.-K. Kim, *Carbon*, 2010, **48**, 1824-1834.
34. R. M. Novais, J. A. Covas and M. C. Paiva, *Composites Part A: Applied Science and Manufacturing*, 2012, **43**, 833-841.
35. S. Jamali, M. C. Paiva and J. A. Covas, *Polymer Testing*, 2013, **32**, 701-707.
36. M. Conceição Paiva, Frank Simon, Rui M. Novais, Tânia Ferreira, M. Fernanda Proença, Wei Xu and Flemming Besenbacher, *ACS Nano*, 2010, **4**, 7379-7386.
37. X. Q. Nguyen and L. A. Utracki, US Patent 5, 451, 106, 19 September 1995 to Nacional Research Council Canada.
38. L. A. Utracki, A. Luciani and D. J. J. Bourry, US Patent 6550956, B1, 2003.
39. I. Alig, P. Pötschke, D. Lellinger, T. Skipa, S. Pegel, G. R. Kasaliwal and T. Villmow, *Polymer*, 2012, **53**, 4-28.
40. C. Vilaverde, R. M. Santos, M. C. Paiva and J. A. Covas, *Composites Part A: Applied Science and Manufacturing*, 2015, **78**, 143-151.
41. D. S. McLachlan, C. Chiteme, C. Park, K. E. Wise, S. E. Lowther, P. T. Lillehei, E. J. Siochi and J. S. Harrison, *Journal of Polymer Science Part B: Polymer Physics*, 2005, **43**, 3273-3287.
42. H. Ago, T. Kugler, F. Cacialli, W. R. Salaneck, M. S. P. Shaffer, A. H. Windle and R. H. Friend, *The Journal of Physical Chemistry B*, 1999, **103**, 8116-8121.
43. T. I. T. Okpalugo, P. Papakonstantinou, H. Murphy, J. McLaughlin and N. M. D. Brown, *Carbon*, 2005, **43**, 153-161.
44. S. Pegel, P. Pötschke, G. Petzold, I. Alig, S. M. Dudkin and D. Lellinger, *Polymer*, 2008, **49**, 974-984.
45. G. R. Kasaliwal, S. Pegel, A. Gödel, P. Pötschke and G. Heinrich, *Polymer*, 2010, **51**, 2708-2720.
46. A. Scurati, D. L. Feke and I. Manas-Zloczower, *Chemical Engineering Science*, 2005, **60**, 6564-6573.
47. N. Domingues, A. Gaspar-Cunha, J. A. Covas, M. Camesasca, M. Kaufman and I. Manas-Zloczower, *International Polymer Processing*, 2010, **25**, 188-198.
48. F. Brochard-Wyart, C. Gay and P. G. de Gennes, *Macromolecules*, 1996, **29**, 377-382.
49. Y. Pan, L. Li, S. H. Chan and J. Zhao, *Composites Part A: Applied Science and Manufacturing*, 2010, **41**, 419-426.
50. C.-R. Yu, D.-M. Wu, Y. Liu, Z.-Z. Yu, A. Dasari, X.-S. Du, Y.-M. Mai, *Composites Science and Technology*, 2011, **71**, 1706-1712.

Preparation of polymer composites with as-produced and chemically functionalised graphite nanoplates: analysis of nanoparticle agglomerate dispersion and re-agglomeration upon relaxation.

